www.cadanda.com
Computer-Aided Design AND APPLICATIONS™

Icing Detection Using Image-based 3D Shape Recovery

Chunsheng Yu[1] and Qingjin Peng[2]

[1]University of Manitoba, umyuc1@cc.umanitoba.ca
[2]University of Manitoba, Pengq@cc.umanitoba.ca

ABSTRACT

Power transmission lines are at risk of the damage when they are exposed to severe ice loads. The accurate detection of ice can reduce the risk to allow ice melting resources to be applied efficiently. Existing methods of the ice detection mainly use the indirect measurement. The ice shape cannot be detected. This paper introduces a new image-based method to detect the ice shape when the ice grows on conductors. The method integrates the technique of camera calibration, image acquisition and 3D shape recovery. It solves the problem of ice detection on severe environments. Experiments show that the proposed method can improve the power system safety significantly.

Keywords: icing detection, 3D shape recovery, power system, image processing.
DOI: 10.3722/cadaps.2010.335-347

1 INTRODUCTION

Power transmission towers may be collapsed if the ice accumulates on power transmission lines. Canada is one of the countries where power transmission lines suffer severe icing problems. For example, the 1998 ice storm caused severe damage to Hydro-Québec's power transmission system. Repair costs after an ice storm can be expensive and electrical outages may deprive residents and businesses of electrical power for extended periods. The ice accumulation detection has drawn a lot of attentions in academic and industrial communities [1].

Ice accretions on transmission lines can vary in geometric shapes based on wind speed, ambient temperature, and the amount of precipitation. When ice accretions are formed, conductors may sway or gallop causing wear and tear on pole cross-arms and associated hardware, or possibly clashing of conductors. A common ice detector is the icing-rate meter (IRM). It is an instrument that detects and measures the icing potential of the air in contact with a probe. When the IRM is installed near a power transmission line, the real-time data on icing rates and the total accumulated weight on a specific line component can be provided. The operator can then assess the risk of overloads of power transmission lines. It therefore gives the operator time to reduce potential damage on the power transmission system. It is a very versatile device that can measure all types of atmospheric icing, whether caused by the passage of cold clouds or by freezing precipitation such as freezing rain or wet snow. Unfortunately, the IRM is unable to detect the ice shape on conductors. The problem is that the detection is on its sensing probe, not directly on power transmission lines.

This research develops an image-based system to monitor ice accretions on power transmission lines. The system monitors the ice shape continuously when the ice grows on power lines. If the ice thickness is greater than a defined threshold, an alarm message will be generated. A decision can then

be made based on the ice status in order to remove the ice on power transmission lines. Fig. 1 shows the proposed system. The system consists of three parts: a) the image capture hardware includes digital cameras and a computer. The computer is used to trigger two cameras to take ice images. The captured images are uploaded automatically to the computer through the USB (universal serial bus) interface; b) the software processes the ice images to obtain the ice shape. The alarm message and ice information are sent to a base station using the wireless network; 3) the base station accepts the alarm message and displays the ice detail to the system user. It can download images and data for the further analysis.

However, detecting the ice shape based on the image information is not an easy task as the ice is transparency or semi-transparency. The image is often affected by the background noise of environments. The noise may deteriorate the performance of image processing. The ice smooth surface also increases the difficulty to find the ice profile on the ice images. We will first review the related research and existing techniques in next section, and then introduce our solutions to the problems.

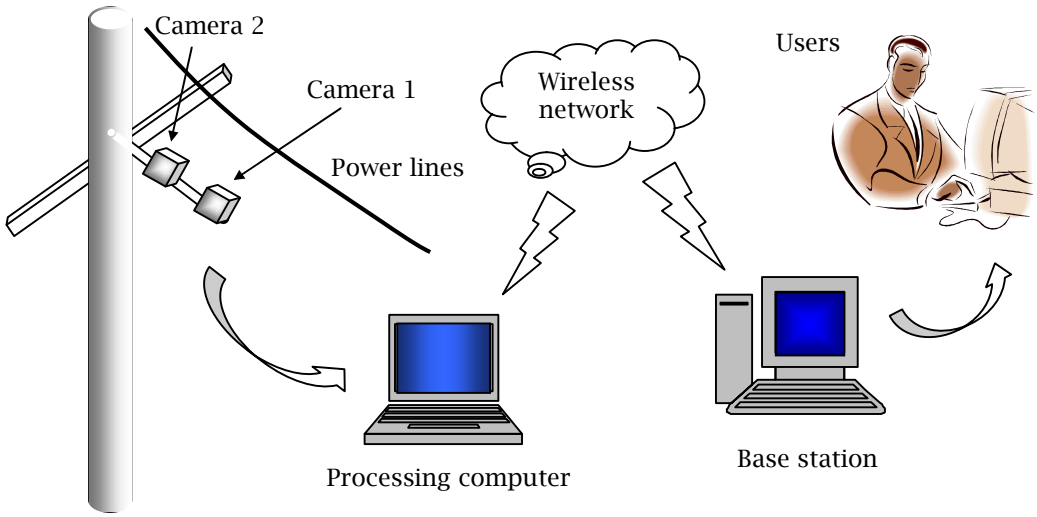

Fig. 1: The proposed ice detection system.

2 RELATED RESEARCH AND EXISTING TECHNIQUES

Vision information has been utilized in the industrial community for a number of years. It has been widely used in product design and manufacturing [2], Robot manipulation [3], 3D object reconstruction [4] and medical processing [5]. There are some image-based research studies on ice monitoring, such as the digital system to characterize frazil in a laboratory environment [6]; using aerial high-resolution digital images tagged by the global positioning satellite (GPS) to identify defects on electric power lines [7]; and using the rough set theory in digital image processing for measuring ice accumulated on power transmission lines [8]. An image-based method for measuring ice accumulation on power transmission lines was developed by Borkowski [8]. The method combines two methods in a non-standard way. One is the δ -mesh method and the other one is the Gouraud shading algorithm. The method has following problems: (a) as the motion of power transmission lines in real environments was not considered, the accurate ice thickness cannot be obtained; (b) it can not automatically detect the edges of ice; and (c) the input image can only contain one power transmission line with a clear background, it fails to detect ice on power transmission lines in complex backgrounds. Although these developments provide useful solutions to the ice control, none of them has been used to monitor the ice accretion in real environments.

Some commercial digital systems have also been reported. Sagometer developed an image-based device to resolve vertical deflection of power lines that is mounted on a transmission tower [9]. There is no function mentioned for the ice detection. Our research aims to accurately monitor ice accretions

using the ice image information. Available techniques of the ice shape reconstruction from 2D images are as follows.

- *Shape-from-shading (SFS):* SFS obtains the 3D shape of an object using the shading information based on the reflected function [10]. The reflection model of the object surface has to be available.
- *Moiré methods*: two gratings are projected onto the object surface to obtain 3D data [11]. The methods have phase discrimination problems when the surface is not smooth. Errors cannot be avoided when the slope of the surface is greater than a limitation.
- *Photogrammetry:* It captures images using multi-cameras. Image coordinates of any feature points in the images can then be measured. There are different strategies and methods using photogrammetry methods [12].
- *Profilometry methods:* include phase-measuring profilometry (PMP) and Fourier transformation profilometry (FTP). PMP projects a fringe pattern onto the object by varying the phase of the pattern. The 3D shape of the object can be recovered by mapping the phase distribution to the height [13]. FTP projects a sinusoidal grating onto the object surface. The 3D shape of the object can be obtained by calculating Fourier transformation of the image, filtering in spatial frequency domain and calculating inverse Fourier transformation [14].

Based on the technical feasibility and the system application environment, the photogrammetry method is used in this research. A major problem using the photogrammetry method in ice shape detection is to find the corresponding points from different images of the same object. A general process of finding corresponding points in the images includes feature extracting and points matching. Feature extracting determines the location and orientation of image features in an image. There are many feature detection algorithms in literature. Corners are the most used features in processing. A template-based method was proposed by Luo *et al* [15]. Corners are considered at saddle points of the magnitude of the vector potential. The junctions of the edge and symmetry lines are defined as corners. An isolated point detection method was described by Gonzalez and Woods [16]. The rate of change of gradient direction and the gradient magnitude are used to detect corner points. Pei and Ding [17] used the sum of the differences to observe the variations along the adaptive vertical and tangent axes. The variations are classified into 36 types. A 'case table' is used to detect the corners. The gradients calculated along x and y-axes, used in many existing algorithms, are not required in this method. The Gabor wavelet was used to detect corners by Gao *et al* [18]. The input image is transformed to several wavelet scales along several directions. The magnitude along a direction that is orthogonal to the gradient orientation is used for the corner measurement. A support vector machine-based algorithm for the corner detection was presented by Banerjee *et al* [19]. A four-dimensional feature vector stores the direction of maximum gray-level change for each edge. The feature vectors are used to detect the corner points.

A comparison of these methods was discussed by Heath *et al* [20]. The conclusion is that there are no significant differences among performances of these methods, therefore the choice of the feature detection algorithm depends on the application. A blob detector was used by Hinz to detect regions on an image [21]. The blob detectors can be grouped into four categories: (1) matched filters/template matching; (2) watershed detection; (3) structure tensor analysis followed by hypothesis testing of gradient directions; and (4) the region detection through a scale-space analysis. Theoretically, the region detection through the scale-space analysis is the most advanced method, and it is often carried out through the computation of local extremes of some normalized derivatives of linear scale-space image representation [22].

Corresponding points matching calculates the similarity of two image feature points. The algorithms of similarity measurement are divided into two categories: area-based matching and feature-based matching [23]. Computing correlation and sum of squared differences (SSD) are the basic techniques for obtaining the correspondence between two or more images [24]. The main problem of the techniques is the size selection of an appropriate window. The window size should be large enough to include enough information of intensity variation, but small enough to avoid the effects of projective distortion. An adaptive window method was proposed by Kanade and Okutomi [25] to select an appropriate window by evaluating the local variation of intensity and disparity. A statistical model of the disparity distribution within the window can then be created. An edge detection-based adaptive window method was proposed by Wang [26]. The window is chosen by the intensity variance without the influence of disparities, therefore the method is robust for variation of intensity.

Using features instead of the intensities allows a representation invariant with respect to distortions resulting from illumination, reflectance or geometry. This makes feature-based algorithms more robust than area-based matching. An algorithm based on a multi-resolution, multiple-hypothesis scheme was designed by Cham and Cipolla [27]. The core of the algorithm is a Bayesian framework for incorporating similarity measurement of feature correspondences in regression. Feature locality and the gray-level gradient associated with the feature were used by Candocia and Adjouadi [28] to measure the similarity of features. Local and global matching strategies are integrated in a matching procedure to ensure that the features are matched with a high degree of similarity. The parallel of epipolar lines were used by Lu and Manduchi [29] as a constraint for feature matching. The algorithm reduces the mismatches and the dimension of search domain.

The preceding research mainly focuses on a general solution of feature detection and feature matching in image processing. None of them has been used to monitor the ice accumulation in real environments. This research proposes a new method to monitor ice accretions on power transmission lines using the image-based shape detection technique. In the following parts of the paper, we will first introduce the proposed ice detection method. The experiment studies are then presented followed by the conclusions and proposed further work.

3 THE PROPOSED ICE DETECTION METHOD

Based on the photogrametry technique, the proposed method uses two ice images to detect the ice shape. The images are taken by two cameras for the same power transmission line. The rotation, translation and intrinsic parameters of the cameras are obtained by a calibration process. As the maximum ice size depends on profile of the ice, the interested corresponding points will only be detected on ice edges on the maximum cross section to simplify the processing. These points will then be used to calculate the maximum ice thickness along a power transmission line. After the edge detection, the peak points on the ice edges can be obtained. Epipolar line and correlation methods are integrated to find the corresponding points of these peak points in the two images. The maximum ice thickness is the distance between two peak points of edges.

In the photogrammetry method, the 3D coordinates of an interesting point on the ice surface are calculated using corresponding points on two images. Therefore the most important step in this method is the point matching algorithm which finds the same interesting point on two ice images. As the ice surface is smooth without special features to be used for matching points in the ice images, the feature-based and area-based points-matching method are combined in this research to provide a solution for the corresponding points matching.

The profile information, epipolar geometry, and edges of the ice images are used to find the search area of corresponding points. The correlation method is used to find the precise position of the corresponding points. A flow chart of the matching processing is shown in Fig. 2. The search area is composed by a group of points around the intersection of epipolar lines and edges. The cross-correlation method calculates the similarity score [16]. In the search area, if the similarity score at one point is greater than a defined threshold then the point is the matching point. An example is shown in Fig. 3. Fig. 4 is a flow chart of the ice detection algorithm. The major steps of the process are system calibration, image data acquisition and ice thickness calculation.

3.1 The System Calibration

In the system calibration, the camera calibration and epipolar geometry calculation are performed. Two types of parameters associated with cameras are determined including intrinsic parameters and extrinsic parameters. The intrinsic parameters include the focal length, principle points and aspect ratio. The extrinsic parameters include the rotation and translation between the camera frame and the 3D world frame. The camera projection matrix is obtained as follows:

$$P = K\left[R^T - R^T t\right] \tag{1}$$

Where $K = \begin{bmatrix} \alpha & \gamma & u_0 \\ 0 & \beta & v_0 \\ 0 & 0 & 1 \end{bmatrix}$ is the intrinsic parameter of a camera, α is scaling factor in x-axes, β is scaling factor in y-axes, γ is the parameter describing the skew of the two image axes and $(u_{0,}v_0)$ is the coordinate pair of the principle point. $R = \begin{bmatrix} r_1 & r_2 & r_3 \end{bmatrix}$ is the rotation matrix from the world system to the camera system, and t is translation vector from the world system to the camera system.

Epipolar geometry is determined by estimating a matrix which describes the projective transformation between the points contained in the images. One of the main problems associated with this approach is the fact that the matrix is sensitive to errors of the point location. The problem is solved using a special designed checkerboard pattern shown in Fig. 5. The use of the checkerboard pattern provides accurate locations of corresponding points in two images because all corresponding points are corners of black and white squares on checkerboard pattern. The corners can be easily extracted from both images [30]. A 8-points algorithm is used to calculate the matrix [31]. The epipolar line $l^{'}$ is calculated after the matrix is obtained.

$$l^{'} = Fx \tag{2}$$

Where F is the matrix and x is a point on the image. The epipolar lines will be used in points matching.

3.2 The Image Data Acquisition

For the image data acquisition, edges of the ice on power transmission lines are extracted from 2D images. A multi-scan method is implemented in the processing. Each image-scanning includes 3 steps: image smoothing, edge detection and edge connection [16]. The iteration numbers of an image-scanning are determined by experiments. After the image-scanning, top and bottom edges of ice on transmission lines are obtained by searching the two longest lines in the images. The intersections of a vertical line with the top and bottom edges are called peak points. There are four pairs of peak points shown in Fig. 6.

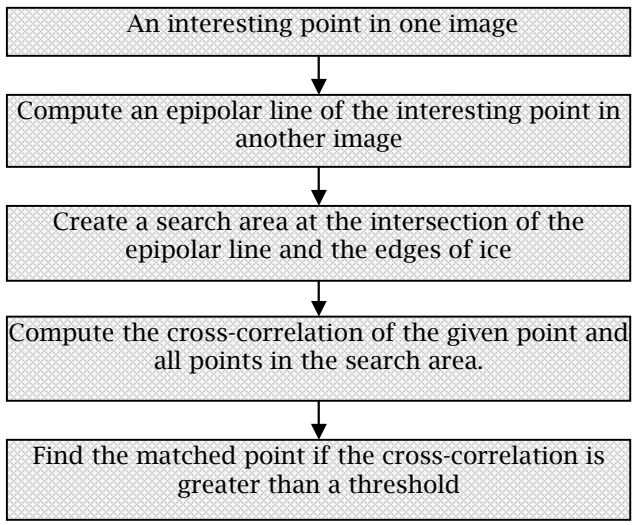

Fig. 2: The workflow of the point matching.

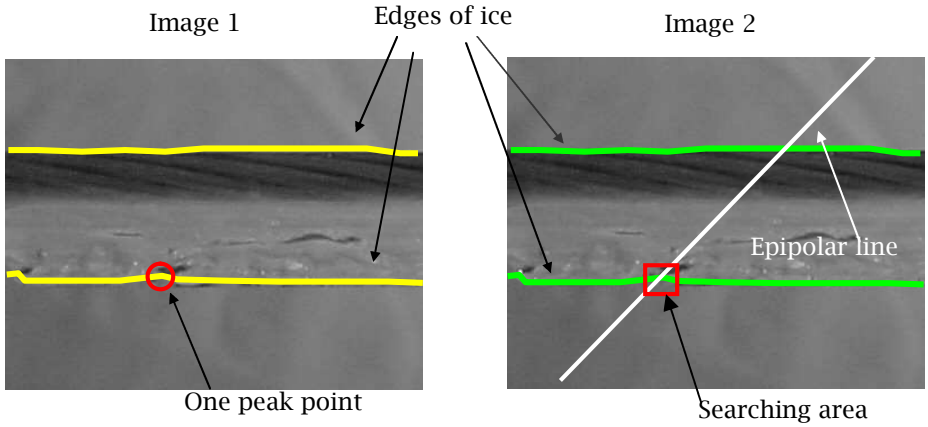

Fig. 3: Feature-based and area-based points matching method.

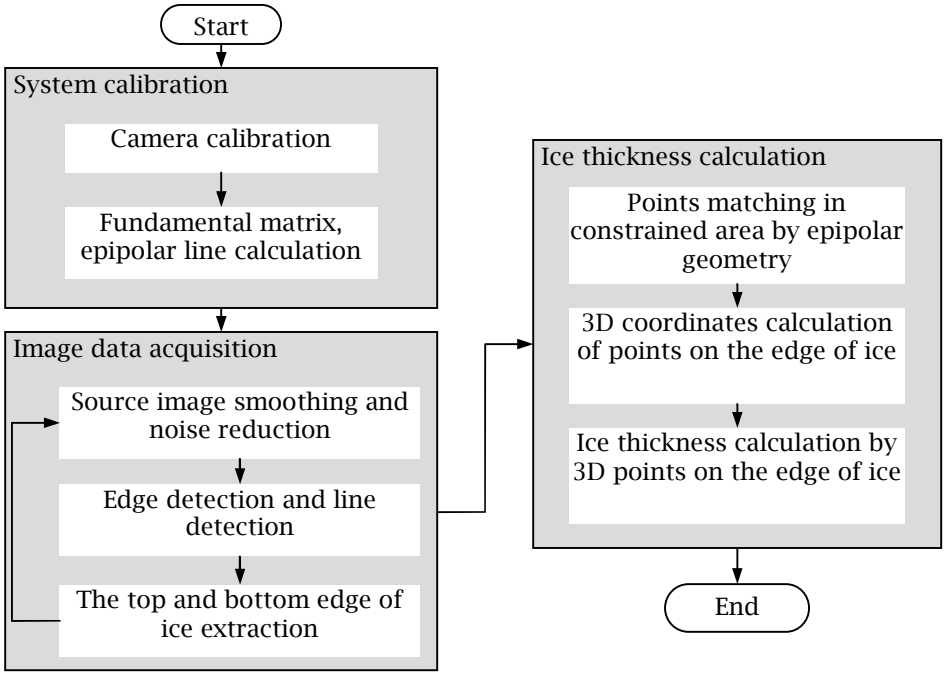

Fig. 4: Flow chart of the ice detection algorithm.

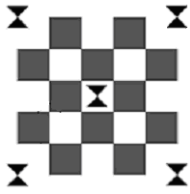

Fig. 5: The special designed checkerboard pattern.

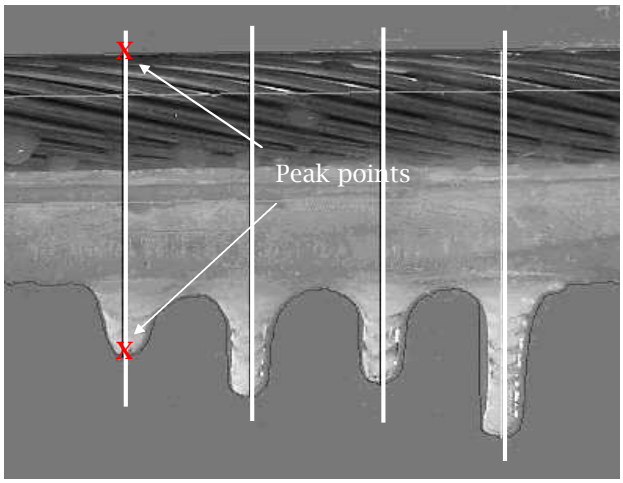

Fig. 6: Peak points on an ice image

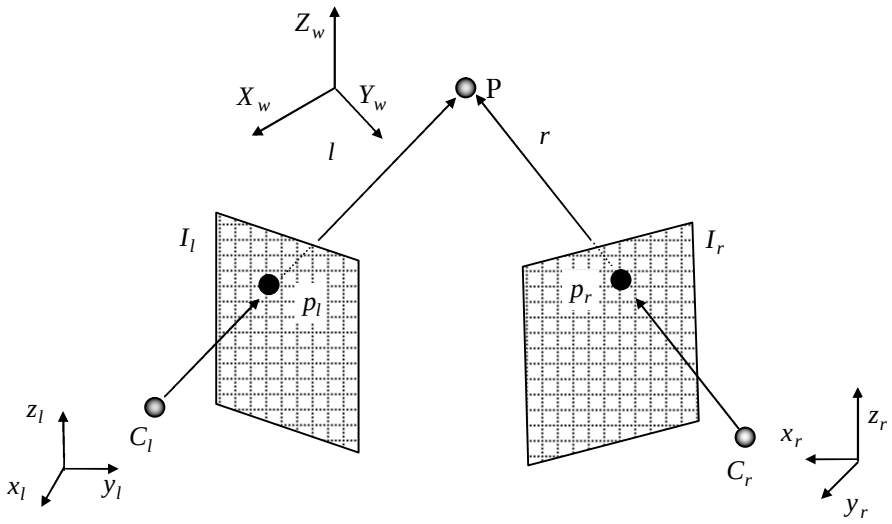

Fig. 7: The geometry of the triangulation method.

3.3 The Ice Thickness Calculation

Fig. 7 shows the geometry of the triangulation method for the ice thickness calculation. $p_l = (x_l, y_l)$ and $p_r = (x_r, y_r)$ are two known image points in the image coordinate system of image planes I_l and I_r. The projective matrix $P = K[R \mid t]$ of the system is known. The 3D coordinates of point P is calculated using these parameters. $[X_w, Y_w, Z_w]$ is the world coordinate system. $[x_l, y_l, z_l]$ and $[x_w, y_w, z_w]$ are the camera coordinate systems of the left and right cameras. C_l and C_r are the optical centers of the left and right cameras. Based on the pinhole model of a camera, the following equations can be obtained [31].

$$\begin{bmatrix} sx_l \\ sy_l \\ s \end{bmatrix} = \begin{bmatrix} P_{l11} & P_{l12} & P_{l13} & P_{l14} \\ P_{l21} & P_{l22} & P_{l23} & P_{l24} \\ P_{l31} & P_{l32} & P_{l33} & P_{l34} \end{bmatrix} \begin{bmatrix} X_w \\ Y_w \\ Z_w \\ 1 \end{bmatrix}$$

and (3)

$$\begin{bmatrix} sx_r \\ sy_r \\ s \end{bmatrix} = \begin{bmatrix} P_{r11} & P_{r12} & P_{r13} & P_{r14} \\ P_{r21} & P_{r22} & P_{r23} & P_{r24} \\ P_{r31} & P_{r32} & P_{r33} & P_{r34} \end{bmatrix} \begin{bmatrix} X_w \\ Y_w \\ Z_w \\ 1 \end{bmatrix} \quad (4)$$

Re-arrange equations (3) and (4),

$$(P_{l11} - P_{l31}x_l)X_w + (P_{l12} - P_{l32}x_l)Y_w + (P_{l13} - P_{l33}x_l)Z_w = P_{l34}x_l - P_{l14} \quad (5)$$

$$(P_{l21} - P_{l31}y_l)X_w + (P_{l22} - P_{l32}y_l)Y_w + (P_{l23} - P_{l33}y_l)Z_w = P_{l34}y_l - P_{l24} \quad (6)$$

and,

$$(P_{r11} - P_{r31}x_r)X_w + (P_{r12} - P_{r32}x_r)Y_w + (P_{r13} - P_{r33}x_r)Z_w = P_{r34}x_r - P_{r14} \quad (7)$$

$$(P_{r21} - P_{r31}y_r)X_w + (P_{r22} - P_{r32}y_r)Y_w + (P_{r23} - P_{r33}y_r)Z_w = P_{r34}y_r - P_{r24} \quad (8)$$

The relation of M, P and B can be expressed as,

$$MP = B \quad (9)$$

where,

$$M = \begin{bmatrix} P_{l11} - P_{l31}x_l & P_{l12} - P_{l32}x_l & P_{l13} - P_{l33}x_l \\ P_{l21} - P_{l31}y_l & P_{l22} - P_{l32}y_l & P_{l23} - P_{l33}y_l \\ P_{r11} - P_{r31}x_r & P_{r11} - P_{r31}x_r & P_{r11} - P_{r31}x_r \\ P_{r21} - P_{r31}y_r & P_{r22} - P_{r32}y_l & P_{r23} - P_{l33}y_r \end{bmatrix} \quad (10)$$

$$P = \begin{bmatrix} X_w \\ Y_w \\ Z_w \end{bmatrix} \quad (11)$$

$$B = \begin{bmatrix} P_{l34}x_l - P_{114} \\ P_{l34}y_l - P_{124} \\ P_{r34}x_r - P_{r14} \\ P_{r34}y_r - P_{r24} \end{bmatrix} \quad (12)$$

The 3D coordinates of point P can be obtained by,

$$P = (M^T M)^{-1} M^T B \quad (13)$$

The ice thickness is finally obtained from the distance between two peak points on the widest outline of the ice edge detected.

4 THE ICE DETECTION SUPPORT SYSTEM

The ice detection system consists of a server, a client and the ice detection process. The client and server architecture of a wireless network system is used as the support system. The ice detection analyzes the captured ice images to obtain the ice size. The server sends commands to the client to

check the current status of ice accumulation, or to retrieve the historical data. The server is located in the users' office. The client receives commands from the server and return ice information to the server.

The ice detection software system is developed using Visual C++. The system detail is shown in Fig. 8. There are five functional programs in the system, the server program, the client program, the ice detection program, and two wireless network threads. The wireless network threads create network connections for the system communication. The wireless network threads constitute separate computational process that runs in parallel with the server and client programs. The advantage of this method is that the wireless network threads may be blocked for waiting for incoming messages, but the server and client programs are still able to continue performing the user's command. The communication among the programs is one of the fundamental problems for implementing the system. To exchange the information between the server and client, a protocol is required to send commands and data over the wireless network. The protocol is designed based on the functions required by the server and the client.

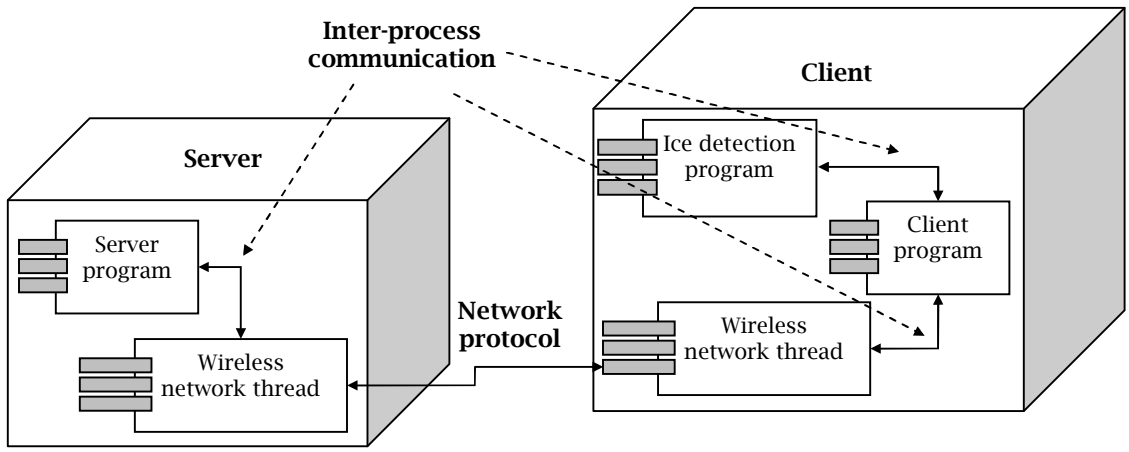

Fig. 8: The support system of the ice detection.

5 EXPERIMENTS OF THE PROPOSED SYSTEM

The experiments of the proposed system include two parts: (a) testing the ice detection method in laboratory, and (b) testing the ice detection system in the real environment. The ice detection system is developed with four modules: the camera calibration, edges of ice detection, points matching based on the epipolar geometry, and 3D coordinates calculation. The advantage of separating the algorithm into different modules is that it makes it possible to test the algorithm for each module at a later stage. The algorithm can be improved by developing a new algorithm for each module without having to redefine whole algorithm. The client side of the ice detection system includes two digital cameras and a laptop computer that are installed on a pole cross-arm. The server side is a desktop computer which is located in a base station.

5.1 Experiments of the Ice Detection Method

Experiments use the 640x480 pixels sized images. The diameter of the transmission line is 16 mm. The planar checkerboard with double-triangle pattern is used for camera calibration. Fig. 9 shows the experimental results of the camera calibration. Fig. 10 is the experimental result of the ice edge detection. Fig. 11 shows the experimental result of the points-matching. One epipolar line and two matched points are shown. Eight peak points on ice edges are marked by numbers. Number 4 is used as an example. The peak point is marked by a dot in left image. The epipolar line of the given point in right image is shown in a black line. The edges of ice are shown in gray lines. The search area for the interesting points in right image is constrained by the epipolar line and ice edges. The black rectangle

in right image is the search area. The matched point is marked by a dot. With the help of the epipolar lines and ice edges, the matched points are found on the smooth surface of ice. The experimental results of the 3D coordinate calculation are shown in Fig. 12. Eight matched points are shown.

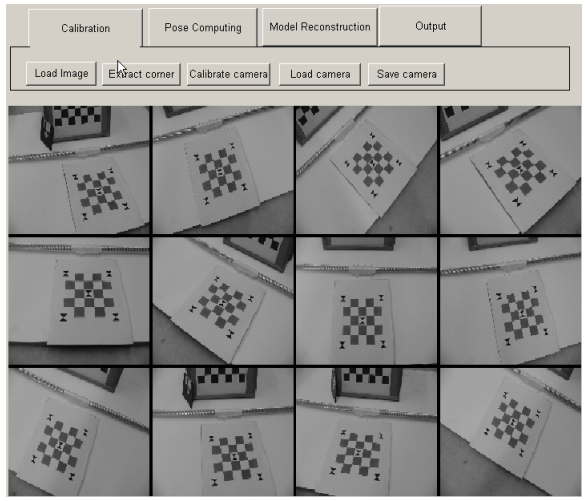

Fig. 9: The camera calibration.

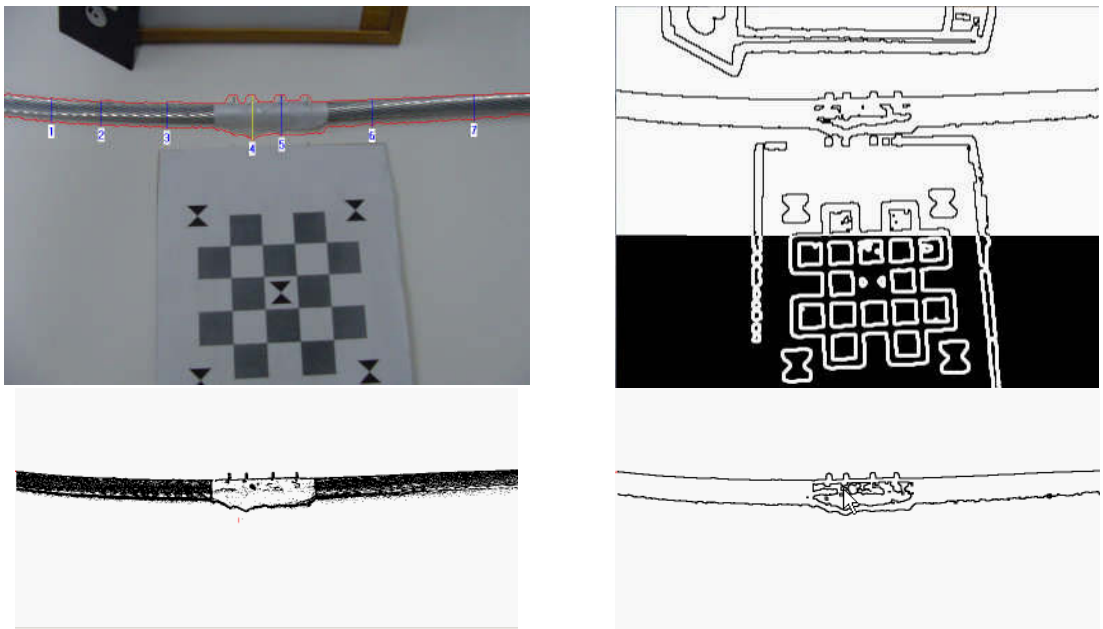

Fig. 10: Multiple scans to detect ice edges.

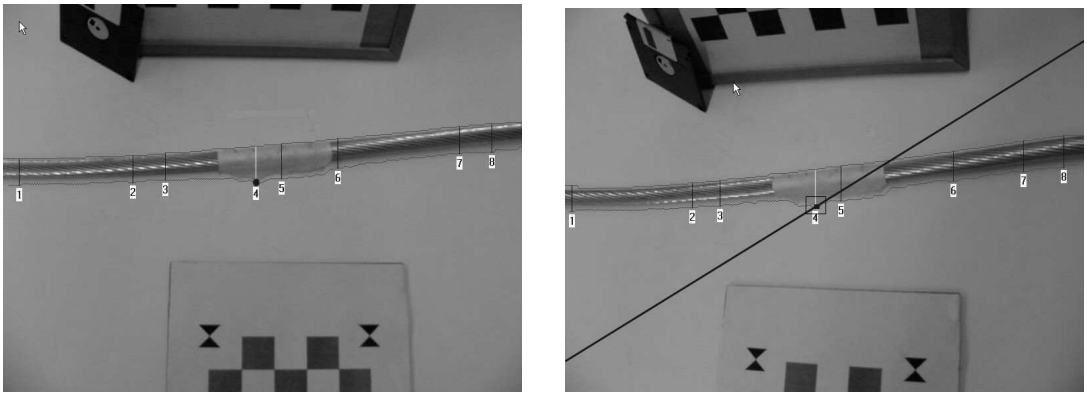

Fig. 11: Epipolar lines in two images.

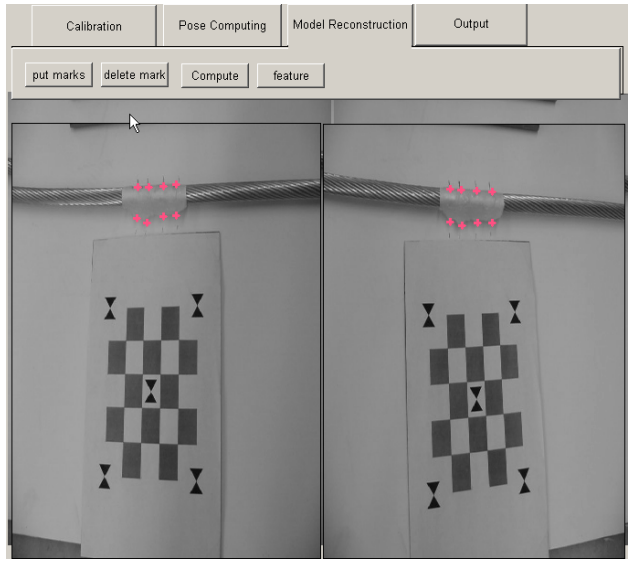

Fig. 12: 3D coordinates of peak points on edges of the ice.

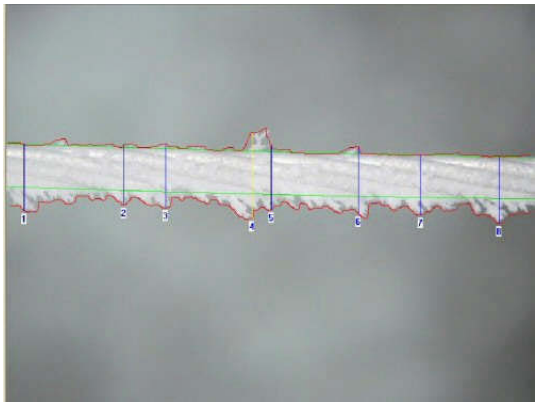

Fig. 12: Hoarfrost on the power transmission line at daytime.

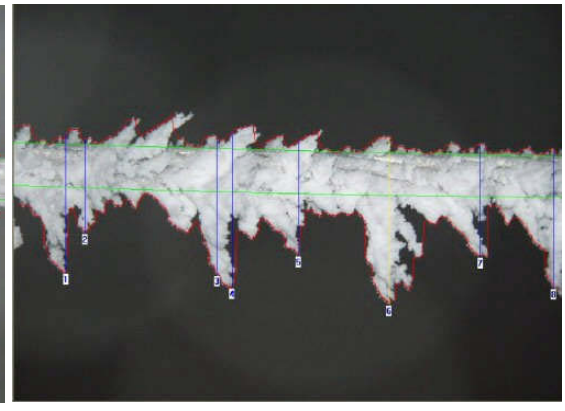

Fig. 13: Hoarfrost on the power transmission line at night.

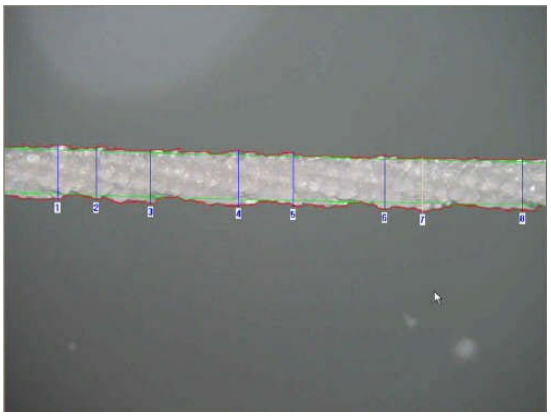

Fig. 15: Ice on the power transmission line at daytime.

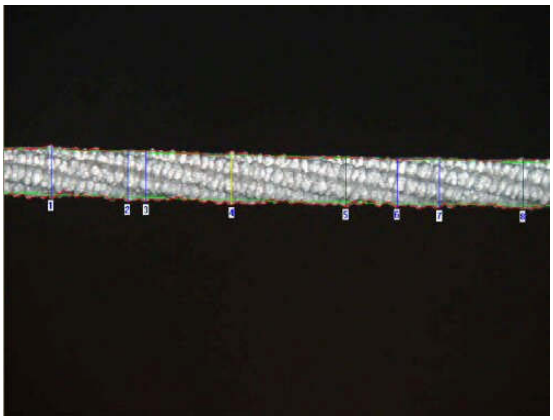

Fig. 16: Ice on the power transmission line at night.

5.2 The Ice Detection System in the Real Environment

In the real environment, the installation distance between the ice detection station and the base station is about 500 meters. The application has validated the ice detection purpose in image processing and signal transfers. Figs 13 -16 show some detected ices in real environments. Figs 13 and 15 are hoarfrosts detected on the power transmission line at daytime. Figs 14 and 16 are ices on the power transmission line at night. Ice sizes are successfully detected for both hoarfrost and ice. The experimental results prove that the ice detection system working in the real environment.

6 CONCLUSIONS AND FURTHER WORK

This research developed a monitoring system for the early detection of ice accretion on power transmission lines to assist in minimizing potential damage cost of power systems. The edge detection, epipolar lines and correlation methods are combined to find the ice size in the proposed ice detection system. The corresponding points were successfully detected on the transparent and smooth ice surface for the ice thickness calculation. This research provides an effective approach to detect ice accretion on power transmission lines. The application shows feasibility of the method in the lab test and real environments.

The pattern recognition will be introduced into the system to efficiently remove the image noise. A knowledge-based ice image database will be built to understand the ice images and to distinguish ice and hoarfrost automatically.

ACKNOWLEDGEMENTS

The authors thank the financial support from Canadian NSERC CRD Grant and Manitoba HVDC Research Centre for this research.

REFERENCES

[1] Savadjiev, K.; Farzaneh, M.: Modeling of Icing and Ice Shedding on Overhead Power Lines Based on Statistical Analysis of Meteorological Data, IEEE Transactions on power delivery, 19(2), 2004, 715-721.

[2] Kim, Y.; Yang, J.; Han, S.: A multichannel visualization module for virtual manufacturing, Computers in Industry, 57, 2006, 653–662.

[3] Jang, H.; Moradi, H,; Minh, P. L.; Lee, S.; Han, J.: Visibility-based spatial reasoning for object manipulation in cluttered environments, Computer-Aided Design, 40, 2008, 422–438.

[4] Hirano, D.; Funayama, Y.; Maekawa, T.: 3D Shape Reconstruction from 2D Images, Computer-Aided Design & Applications, 6(5), 2009, 701-710.

[5] Yau, H. T.; Lin, Y. K.; Tsou, L. S.; Lee, C. Y.: An Adaptive Region Growing Method to Segment Inferior Alveolar Nerve Canal from 3D Medical Images for Dental Implant Surgery, Computer-Aided Design & Applications, 5(5), 2008, 743-752.
[6] Doering, J. C.; Morris, M. P.: A digital image processing system to characterize frazil ice, Canadian Journal of Civil Engineering, 30(1), 2003, 1-10.
[7] Ostendorp, M.: Innovative airborne inventory and inspection technology for electric power line condition assessments in remote areas and cold climates, Proceedings of the International Conference on Cold Regions Engineering, 1999, 805-811.
[8] Borkowski, M.: Digital image processing in measurement of ice thickness on power transmission lines: a Rough Set approach. Thesis (M.Sc.), University of Manitoba, 2002.
[9] Edllink, http://www.edmlink.com/products.html#SG, Saometer.
[10] Roman, D.; Basri, R.: Statistical Symmetric Shape from Shading for 3D Structure Recovery of Faces, 8th European Conference on Computer Vision, 2004, 99-113.
[11] Chen, F.; Gordon, M. B; Song, S.: Overview of three-dimension Shape Measurement Using Optical Methods, Optical Engineering, 39, 2000, 10-22.
[12] Salvimas, J.: An Approach to Coded Structured Light to Obtain Three Dimensional Information, Ph.D. Thesis, University of Gerona, 2001.
[13] Quan, C.; He, X. Y.: Shape measurement of small objects using LCD fringe projection with phase shifting, Optics Communications, 2001, 21-29.
[14] Su, X.; Chen, W.: Fourier transform profilometry: a review, Optics and lasers in Engineering, 35, 2001, 263-284.
[15] Luo, B.; Cross, A.D.J.; Hancock, E.R.: Corner detection using vector potential, Fourteenth International Conference on Pattern Recognition, 2, 1998, 1018-1021.
[16] Gonzalez, R.C.; Woods, R.E.: Digital Image Processing, 2nd edition, Prentice Hall, 2002.
[17] Pei, S.; Ding, J.: New corner detection algorithm by tangent and vertical axes and case table, IEEE International Conference on Image Processing, 1(11-14), 2005, I-365-8.
[18] Gao, X.; Sattar, F; Venkateswarlu, R.: Corner detection of gray level images using Gabor wavelets, International Conference on Image Processing, 4(24-27), 2004, 2669-2672.
[19] Banerjee, M.; Kundu, M.K.; Mitra, P.: Corner detection using support vector machines, Proceedings of the 17th International Conference on Pattern Recognition, 2(23-26), 2004, 819 - 822.
[20] Heath, M.D.; Sarkar, S.; Sanocki, T.; Bowyer, K.W.: A robust visual method for assessing the relative performance of edge-detection algorithms, IEEE Transactions on Pattern Analysis and Machine Intelligence, 19(12), 1997, 1338 - 1359.
[21] Hinz, S.: Fast and subpixel precise blob detection and attribution, IEEE International Conference on Image Processing, 13(11-14), 2005, III - 457-60.
[22] Damerval, C.; Meignen, S,: Blob Detection With Wavelet Maxima Lines, IEEE Signal Processing Letters, 14(1), 2007, 39 - 42.
[23] Li, G.; He, Y.: A hierarchical combined feature and area-based stereo matching algorithm, IEEE International Symposium on Circuits and Systems, 2(26-29), 2002, II-277- II-280.
[24] Vincent, E.; Laganiere R.: An Empirical Study of Some Feature Matching Strategies, The 15th International Conference on Vision Interface, http://www.cipprs.org/vi2002, 2002.
[25] Kanade, T.; Okutomi, M.: A stereo matching algorithm with an adaptive window: theory and experiment, IEEE Transactions on Pattern Anal. and Machine Intelligence, 16(9), 1994, 920-932.
[26] Wang, K.: Adaptive stereo matching algorithm based on edge detection, International Conference on Image Processing, 2(24-27), 2004, 1345 - 1348.
[27] Cham, T.; Cipolla, R.: A statistical framework for long-range feature matching in uncalibrated image mosaicing, IEEE Conference on Computer Vision and Pattern Reco., 23-25, 1998, 442 - 447.
[28] Candocia, F.; Adjouadi, M.: A similarity measure for stereo feature matching, IEEE Transactions on Image Processing, 6(10), 1997, 1460 - 1464.
[29] Lu, X.; Manduchi, R.: Wide baseline feature matching using the cross-epipolar ordering constraint, Proceedings of IEEE Conference on Computer Vision and Pattern Recognition, 1, 2004, I-16 - I-23.
[30] Yu, C.; Peng, Q.: Robust recognition of checkerboard pattern for camera calibration, Journal of Optical Engineering, 45(9), 2006, 093201-(1-9).
[31] Hartley, R.; Zisserman, A.: View Geometry in Computer Vision, 2nd edition, Cambridge University Press, 2004.